The International Journal of Advanced Manufacturing Technology (2018) 99:1283–1291
https://doi.org/10.1007/s00170-018-2546-0

ORIGINAL ARTICLE

Jet properties and mixing chamber flow in a high-pressure abrasive slurry jet: part I—measurement of jet and chamber conditions

Michael Teti [1] · Marcello Papini [1,2] · Jan K. Spelt [1,2]

Received: 10 April 2018 / Accepted: 10 August 2018 / Published online: 21 August 2018

Abstract
Techniques to enhance the performance of a high-pressure abrasive slurry jet micro-machining process (HASJM) were investigated by altering the conditions within the jet. The slurry flow rate was controlled using six inlet tubes (cross-sectional areas of 0.2, 0.46, 1.27, 1.77, 3.08, and 4.51 mm^2), and was found to have a large effect on the conditions within the mixing chamber. The tubes permitted the use of high-concentration slurry solutions, which resulted in increased machining rates and the ability to machine glass targets without cracking by using a minimum particle concentration of 17 wt%. Slurry tubes producing large slurry flow rates caused the mixing chamber to flood, resulting in a much lower jet velocity. The size of the smallest slurry tube size that caused the mixing chamber to flood was dependent on the pump operating pressure, and varying from 1.27 mm^2 at 134 MPa, to 1.5 mm^2 at 233 MPa. Mixing chamber flooding significantly reduced the erosion rate of the jet and increased the machining time, as discussed in the second part of this two-part paper. Mixing chamber pressures were found to be low enough to cause boiling, which increased the jet diameter and the width of features that could be machined without a mask.

Keywords Abrasive slurry jet · Slurry entrainment · Micro-machining · Mixing chamber

1 Introduction

Abrasive slurry-jet micro-machining (ASJM) has seen rapid development in the recent past as a cost-effective and versatile means of machining a wide range of materials, including those that are difficult to cut using more common processes. For example, Kowsari et al. [1] machined fine features in sintered ceramics using a low-pressure abrasive slurry jet, typically operating at less than 14 MPa. Liu [2] investigated a similar process using abrasive water jet micro-machining (AWJM) fitted with micro-nozzles. A main advantage of ASJM and AWJM over traditional cutting with tools is their versatility. They can drill, mill, and cut essentially any material without changing tools and without tool wear. Abrasive water and slurry jets also have the advantage of avoiding damage caused by frictional tool heating [3].

At low operating pressures, ductile erosion is dominant, which can lead to irregular machining. For example, operating a slurry jet at 3 MPa, Nguyen et al. [4] reported machining holes with "W"-shaped cross-sections, while Wang et al. [5] found that the "W"-shaped cross-sections could be avoided by increasing the operating pressure of the jet. Pang et al. [6] found wavy patterns in channels machined at 14 MPa due to an insufficient particle kinetic energy. A jet impinging perpendicular to the workpiece will result in fluid streamlines that abruptly change direction radially around the stagnation zone. As discussed by Humphrey [7], particles will follow the fluid streamlines and are carried away from the center of the jet when the particle Stokes number is less than about one. For low-pressure abrasive slurry jet machining, Nouraei et al. [8] found that particles continued to accelerate after exiting the nozzle and traveled slower than the surrounding water in the jet. They found that increasing the standoff distance increased the velocity (and thus Stokes number) so that W-shaped cross sections could be avoided.

Attempts to raise the operating pressure of pre-mixed ASJM systems to increase erosion rates have resulted in slurry

✉ Marcello Papini
mpapini@ryerson.ca

✉ Jan K. Spelt
spelt@mie.utoronto.ca

[1] Department of Mechanical and Industrial Engineering, University of Toronto, 5 King's College Road, Toronto, ON M5S 3G8, Canada

[2] Department of Mechanical and Industrial Engineering, Ryerson University, 350 Victoria Street, Toronto, ON M5B 2K3, Canada

valves becoming prematurely damaged [9] and large rates of wear within the nozzle [10]. In these systems, the slurry tank is pressurized and a valve is used to start and stop the high-pressure slurry flow [11]. Miller [11] explained that eliminating the valve by using the pump to start and stop the jet could waste up to 99% of the pumping energy and increase the machining time.

Abrasive water jet micro-machining (AWJM) can create much faster abrasive jets, because dry particles are introduced to the water jet in a mixing chamber along with air. Haghbin et al. [12] investigated the effect of this entrained air in the water jet and found it to increase both the erosion rate and waviness of machined channels. They also reported that air caused the jet to spread at a larger rate, increasing the width of the channels [13].

Haghbin et al. [12] modified an AWJM system to feed a slurry of water and abrasive into the mixing chamber where it combined with the high-pressure jet of water before exiting through the mixing tube. This eliminated the entrained air and created a high-pressure abrasive slurry jet micro-machining (HASJM) system that did not rely on a pressurized premixed slurry with its associated valve wear. HASJM has a much greater erosion rate than the lower pressure ASJM, but it produces wider jets. When compared to AWJM, Haghbin et al. [14] found that HASJM created 26% narrower features due to the decrease in jet divergence caused by the elimination of the entrained air. The waviness of channels machined with HASJM was also found to decrease by 3.4 times compared to AWJM, because of a lower variation in the abrasive mass flow rate. A limitation of the HASJM system was the needle valve used to regulate the slurry flow rate into the mixing chamber, which was only capable of regulating flows with particle concentrations of 6 wt% or less, and had a tendency to clog.

Haghbin et al. [12] reported that the mixing chamber in their HASJM system could become flooded when the mass flow rate of slurry into the mixing chamber exceeded that exiting. Such flooding resulted in a marked reduction in particle velocity exiting the jet [13]. However, the process conditions leading to this flooding condition were not well-defined. They reported that the greatest erosion rate occurred when the slurry flow rate into the mixing chamber was just below the rate that was suspected of causing flooding [12].

The main objectives of the present study were to increase the machining efficiency in HASJM by optimizing the slurry inlet conditions to maximize the erosion rate of the jet, and to minimize the diameter of the abrasive jet to permit the machining of smaller features. The present paper describes experiments that were made to understand the conditions within the mixing chamber and mixing tube where the slurry is entrained by the high-pressure water jet exiting the orifice. The accompanying paper [15] describes the computational fluid dynamics (CFD) modeling of the processes within the mixing chamber and mixing tube, and presents the results of machining experiments which quantified the jet erosion rate in the fabrication of milled holes and channels in aluminum.

2 Theory

2.1 Effect of slurry flow rate

A schematic of the HASJM set-up is shown in Fig. 1, where $\dot{m}_w$ and $\dot{m}_s$ represent the mass flow rates of water and slurry, respectively, $\dot{m}_T$ is the total mass flow rate exiting the mixing tube, and Δh is the elevation of the slurry tanks. The apparatus is described in more detail in Section 3.1, and was similar to that used by Haghbin et al. [12], who explained how the high-velocity jet of water from the orifice created a vacuum within the mixing chamber that was proportional to the jet velocity and hence to the pump pressure. The pressure difference between the mixing chamber and the upper slurry tank was the main driving force for the slurry flow rate, and was controlled by using slurry inlet tubes of various diameters.

The water velocity through the orifice was related to the pump pressure, P, according to the relation [16].

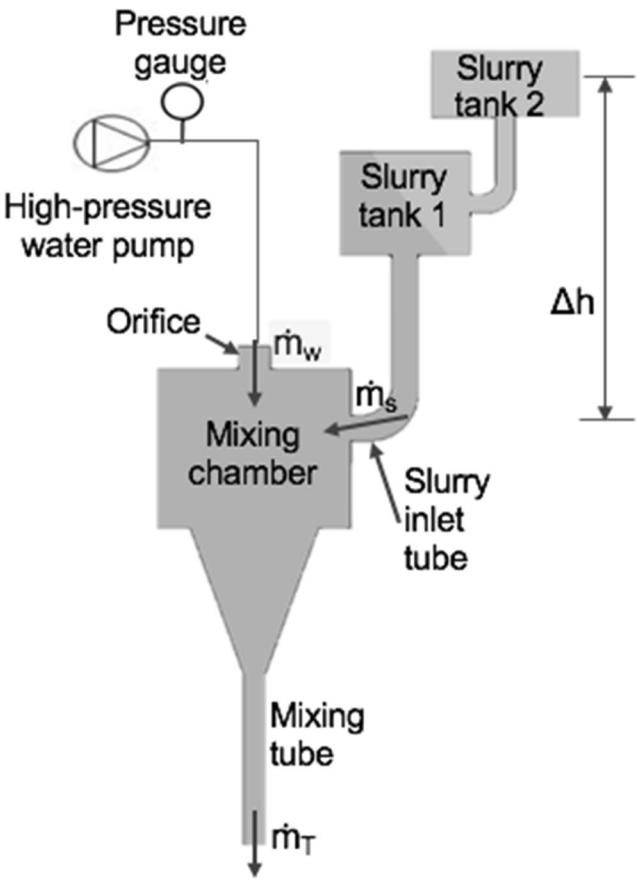

Fig. 1 Schematic of HASJM set-up. Figure is not to scale

$$v_o = \mu\sqrt{\frac{2P}{\rho_w}} \quad (1)$$

where v_o is the velocity from the orifice, μ is the orifice efficiency, and ρ_w is the density of water.

2.1.1 Jet diameter

Haghbin et al. [12] reported that the air entering the mixing chamber with the abrasive in AWJM caused the jet divergence angle to increase from 1.5° in HASJM to 6.9° in AWJM. This effect can also be seen by comparing a water-only jet, achieved by blocking the abrasive inlet to the mixing chamber, to a jet entraining air within a mixing chamber that was open to the atmosphere, as displayed in Fig. 2.

It can be seen that the jet diameter was smaller in the water-only condition when air entrainment was minimal and was less than the diameter of the mixing tube (Fig. 2). This effect of air entrainment within a liquid jet traveling through air can be understood in terms of three regions of flow development as described by Leu et al. [16] and Huang et al. [17]. The initial region is the potential core, where very little surrounding air is entrained by the jet, the water velocity is constant, and the jet does not spread.

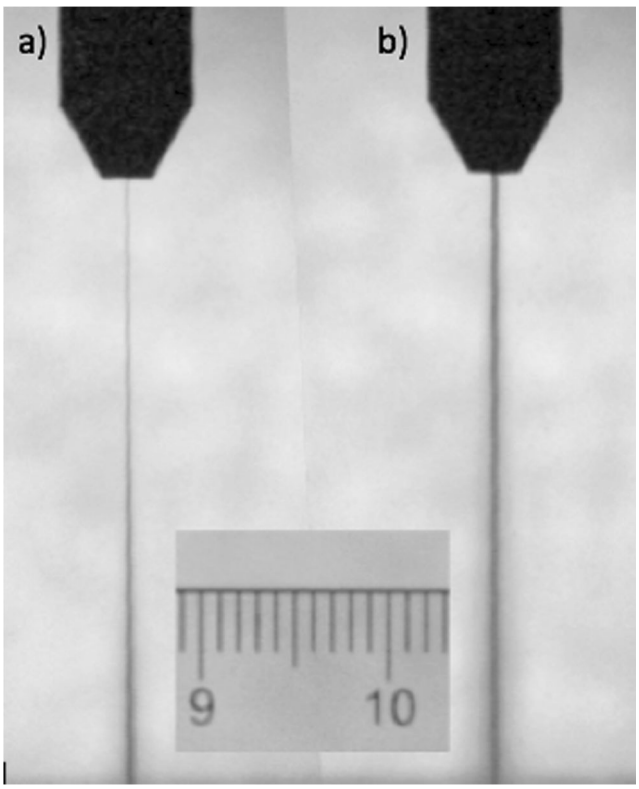

Fig. 2 Diameter of: (**a**) water-only jet, and (**b**) jet with entrained air using a pump pressure of 233 MPa. Scale in mm

Further downstream, air entrainment grows and the water velocity begins to decrease as the jet spreads and becomes turbulent and surrounded by mist. The final region is known as the diffused droplet region where the jet divergence and air entrainment reach a maximum. In the present study, when the mixing chamber was open to the atmosphere, the jet exiting the orifice was initially smaller than the mixing tube, but the mixing chamber was sufficiently long to cause significant air entrainment so that the jet spread to the mixing tube diameter (Fig. 2b). In the water-only condition, however, the slurry inlet was sealed so that relatively little air surrounded the jet and its diameter remained smaller than that of the mixing tube, as seen in Fig. 2a, consistent with the observations of Haghbin et al. [12] using HASJM.

3 Experiments

3.1 HASJM apparatus

The HASJM apparatus was similar to the system used by Haghbin et al. [12], which was based on an OMAX 2626 Jet Machining Center (OMAX Corp., Kent, Washington, USA). This AWJ system was capable of supplying pump pressures up to 345 MPa and was used with a diamond, 127 μm diameter orifice and a tungsten carbide, 254 μm diameter mixing tube. The positioning accuracy of the jet was 76 μm over 30 cm. A diagram of the system and description of its components can be found in [18].

High-pressure water was pumped through the orifice into the mixing chamber where it combined with a premixed slurry that entered from the abrasive inlet before exiting through the mixing tube, as shown in Fig. 1. The slurry flow rate was determined by a combination of the strong suction pressure created within the mixing chamber, the elevation of the slurry tanks, Δh, and the flow resistance created by the slurry tubes of varying inner diameters. Six slurry tube sizes were used having cross-sectional areas of 0.2, 0.46, 1.27, 1.77, 3.08, and 4.51 mm^2. The same dual slurry tank arrangement and stirring mechanism was used as Haghbin et al. [12], with the height difference between the upper slurry tank and the slurry inlet fixed at 1 m for all experiments. The elimination of the slurry control valve used in their system prevented the build-up of particles in the valve and permitted the use of much higher particle concentrations.

All experiments used a water-based slurry containing 320 mesh garnet particles (Barton International, Glens Falls, NY, USA) with an average diameter of 38 μm. The use of approximately the same particle size distribution in each experiment was ensured by using the ASTM quartering technique to sample the powders [19].

3.2 Measurements

3.2.1 Mass flow rate

The slurry mass flow rates were measured using the difference in weight of the slurry tank before and after running a timed experiment. Tests were run four times for each of the six slurry tube sizes using a mass balance that gave an accuracy of ±0.5 g/min. The mass flow rate of water supplied by the pump through the orifice was measured using the same balance during a timed experiment in the water-only condition where the slurry inlet was blocked and the end of the mixing tube was attached to a copper pipe leading to a closed container of cold water. Sealing the copper tube to the end of the mixing tube ensured that all mist and any possible water vapor generated by boiling (discussed in Section 3.2.2) condensed in the pool of cold water.

3.2.2 Mixing chamber pressure, slurry temperature, jet diameter, and particle concentration

The pressure within the mixing chamber was measured using a pressure gauge (WIKA type 213.53, WIKA Instruments Ltd., Edmonton, Alberta, Canada) having an accuracy of ± 2.5% attached to a T-connector on the slurry tube adjacent to the mixing chamber. All connections were sealed with vacuum grease.

The temperature of the slurry exiting the mixing tube was measured using a thermometer placed in an insulated container that collected the slurry. Tests showed that this temperature did not change when the mixing chamber was insulated, indicating that adiabatic conditions could be assumed so that the slurry exit temperature was also that within the mixing chamber. These data were used to assess the likelihood of boiling within the mixing chamber.

The jet diameter was measured as the width of a machined slot made at a slow traverse speed of 10 mm/min in a 2-mm-thick polymeric foam board (Renshape, Huntsman Advanced Materials, Salt Lake City, UT, USA). The foam eroded rapidly under these conditions so that the cut width, measured using a microscope and image analysis, provided a good estimate of the jet diameter. As an additional confirmation of jet diameter, images of the jet were captured using a digital camera (EOS Rebel T6, 18 megapixels, EF-S 55–250 mm 1:4–5.6 IS STM zoom lens, Canon, Tokyo, Japan).

Blind holes were machined on aluminum alloy 6061-T6 [20] to examine the effect of particle concentration on centerline depth. Holes and channels were machined on borosilicate glass (Borofloat, Schott Inc., NY, USA; SiO_2 81 wt%, B_2O_3 13 wt%, Na_2O/K_2O 4 wt%, Al_2O_3 2 wt% [21]) at various particle concentrations to assess the ability of the HASJM system to avoid cracking while machining brittle materials. The mechanical properties of the target materials are shown in Table 1. Haghbin et al. [14] studied the effects of particle velocity on the material removal rates of these target materials using a slurry jet. Hole and channel profiles from the experiments were examined using an optical profilometer (ST400, Nanovea Inc., Cal, USA) having a depth resolution of 0.1 μm. Further machining experiments are described in Part II of the paper [15].

4 Results and discussion

This section describes the results of a series of experiments that were aimed at understanding the conditions within the HASJM mixing chamber that affected the jet diameter, velocity, and material removal rate.

4.1 Effect of slurry flow rate

4.1.1 Particle concentration

Particle concentration contributes to the total mass flow rate of abrasives exiting the mixing tube, thus affecting the rate of target material removal for a given particle velocity, as described by the specific erosion rate, E, defined as the mass of target material removed, M_m, divided by the mass of abrasive used, M_a ($E = M_m/M_a$). Figure 3 shows the effect of inlet particle concentration on the centerline depth of blind holes in 6061-T6 for two inlet slurry tube sizes.

For a given tube size, the hole depth increased significantly as the inlet particle concentration increased. For a given concentration, the hole depth at a given dwell time also increased as the tube size decreased, because, as will be seen in the accompanying paper [15], the particle velocity increased. Eliminating the slurry valve used by Haghbin et al. [12] in favor of controlling the slurry flow rate using tubes of different diameters thus increased the machining rate by permitting the use of slurry solutions with greater than 6 wt% of abrasive. Figure 3 shows that rate of change of the hole depth tended to decrease as the holes became deeper. This was due to the increasing depth of the stagnation zone at the bottom of the holes, and will be discussed further in the companion paper [15].

In addition to increasing the erosion rate, the use of relatively high particle concentrations has been found to be useful in the machining of glass [24], where the relatively large

Table 1 Mechanical properties of target materials

	Glass [22]	AA6061-T6 [23]
Density (g/cm^3)	2.23	2.7
Young's modulus (GPa)	64	68.9
Poisson's ratio	0.2	0.33
Knoop hardness (MPa)	480	120

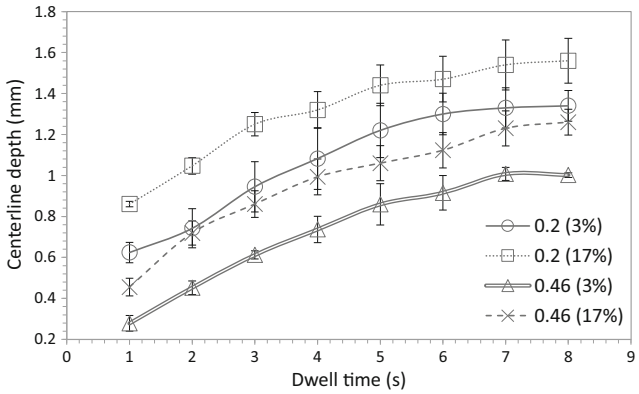

Fig. 3 Centerline depth of blind holes in aluminum 6061-T6 at two inlet slurry particle concentrations for each of two slurry tube diameters. Pump pressure of 203 MPa. The legend gives the slurry tube cross-sectional area (mm^2) with the inlet particle concentration in weight %. Scatter bars represent ±1 standard deviation provided by three repeat tests. The lines are to guide the eye

velocities of HASJM and AWJM can make it difficult to avoid cracking. Huang et al. [17] suggested that the initial impact on a workpiece produces a very large water hammer pressure that generates a shock wave which propagates through the workpiece and has the ability to crack and plastically deform the materials. Schwartzentruber and Papini [25] were able to reduce chipping in a glass target in AWJM by securing a feeler gauge over the workpiece to act as a shield during the initial jet impact.

The present HASJM system was used to machine blind holes and channels in soda lime glass at an operating pressure of 134 MPa with varying inlet particle concentrations. Low particle concentrations were frequently observed to cause significant cracking damage to the glass workpiece. For example, Fig. 4 shows that blind holes machined using 9 wt% particle concentration (Fig. 4a) experienced a large amount of cracking at the edge of the hole, while there was essentially no cracking when 17 wt% slurry was used (Fig. 4b). It is noted that the horizontal bands extending from either side of each hole are very shallow channels (less than 4 μm deep) created by the jet as it rapidly traversed to the hole location. Stagnation pressures are known to build-up at the bottom of blind holes, which results in cracking and chipping of a brittle workpiece [24]. Liu and Schubert [24] demonstrated that a reduction in the stagnation pressure occurs when entraining powder within an AWJM system because the kinetic energy of the water is consumed accelerating the particles. Therefore, it is hypothesized that the higher particle concentrations in Fig. 4b decreased the stagnation pressure to the point where material was removed before cracking could occur.

4.1.2 Slurry tube size

Figure 5 shows that large changes in the slurry mass flow rates were obtained by varying the size of the slurry tube connected to the mixing chamber, and that the nature of the changes depended on whether the mixing chamber was flooded (i.e., filled with slurry). Although the flow in the mixing chamber could not be observed directly, evidence for flooding came from the trend of the slurry mass flow rate in Fig. 5 and from the pressure in the mixing chamber, discussed in Section 4.2.1. Flooding was also predicted by the CFD models of the second part of this paper [15], and these predictions of the fully-flooded condition (mixing chamber completely filled with slurry) are shown as the two vertical lines on Fig. 5.

For tube sizes smaller than those predicted to cause mixing chamber flooding by the accompanying CFD model (the vertical lines), Fig. 5 shows that the slurry mass flow rate increased as the size of the slurry tube increased. When the slurry flow rate became large enough to flood the mixing chamber, the slurry flow rate fell to become approximately constant, changing very little with increasing tube size, in agreement with the findings of Haghbin et al. [12]. As will be discussed in Section 4.2.1, this decrease in the slurry flow rate was caused by a decrease in the suction in the flooded mixing chamber. For the data of Fig. 5, the ratio of the slurry flow rate to the flow rate of water through the orifice ranged from 5% for the smallest slurry tube to 77% for the largest tube.

The three smallest tube sizes in Fig. 5 show that the higher pump pressure caused a slightly larger slurry flow rate before flooding, because the higher jet velocity from the orifice produced a lower mixing chamber pressure by extracting more air, causing a small (15% average) increase in the slurry mass

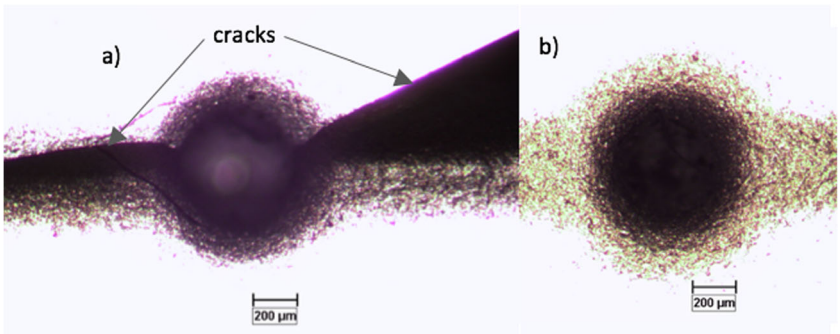

Fig. 4 Microscope images of the surface region around blind holes machined in glass using (**a**) 9 wt%, and (**b**) 17 wt% particle concentrations at the slurry inlet with a pump pressure of 134 MPa

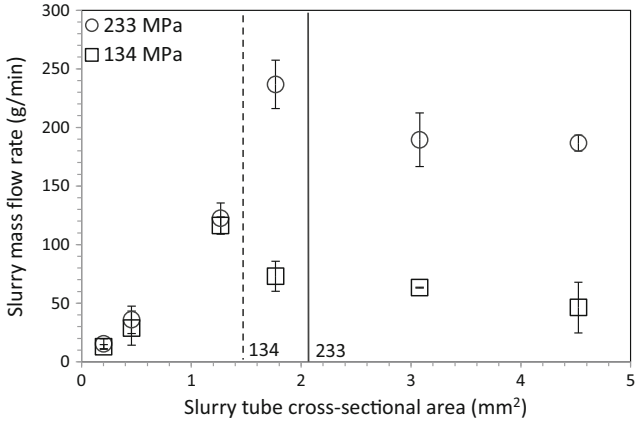

Fig. 5 Effect of the tube size on the slurry mass flow rate entering the mixing chamber measured at two pump pressures. The solid and dashed vertical lines indicate the fully-flooded conditions for 233 MPa and 134 MPa, respectively, as predicted by the CFD model [15] (mixing chamber flooding to the right of the lines). Scatter bars represent ± 1 standard deviation from four separate tests

flow rate between 233 and 134 MPa. After flooding, the effect of pump pressure on the slurry flow rate was much larger, as discussed in Section 4.1.3.

Slurry flow could also be controlled by varying the height difference between the mixing chamber and the slurry tank, but all mass flow rate experiments were conducted with the slurry tank located 1 m above the height of the jet. Making the slurry tank level with the mixing chamber caused the mass flow rates to decrease by an average of 21% for each slurry tube, for cases in which the mixing chamber was not flooded.

4.1.3 Flooding condition

The vertical lines on Fig. 5 represent the mixing chamber fully-flooded condition at each specified operating pressure, as predicted using the CFD model [15]. When the mixing chamber was fully flooded, it was completely filled with liquid, and after this point the slurry mass flow rates dropped, becoming approximately constant at approximately 60 g/min and 200 g/min for pump pressures of 134 MPa and 233 MPa, respectively, i.e., a slurry mass flow rate increase of 233% due to the increase in pump pressure. In the fully-flooded condition, the jet of water from the orifice immediately penetrated the slurry in the mixing chamber and experienced a sharp decrease in velocity, effectively acting as a submerged jet entraining slurry into the mixing tube, i.e., traveling through high-density slurry instead of air. The effect of flooding on the jet velocity and the overall jet performance is described in the accompanying paper [15]. A larger pump pressure increased the velocity of the jet as it penetrated the slurry pool, thereby entraining more slurry into the mixing tube. Therefore, as seen in Fig. 5 the full flooding condition at 233 MPa required a larger tube size and slurry flow rate than at 134 MPa.

4.2 Jet diameter and machined feature width

4.2.1 Boiling

The possibility of liquid boiling within the mixing chamber was examined by measuring the temperature and pressure of the slurry for each of the slurry tube sizes and the water-only condition (tube size of zero) as shown in Fig. 6.

The vertical line of Fig. 6 marks the onset of boiling within the mixing chamber, where the vapor pressure of water at the chamber temperature equaled the measured pressure. The tube sizes to the left of the vertical line produced mixing-chamber pressures that were lower than the vapor pressure of water and were thus predicted to cause slurry boiling. The water-only condition (zero tube size, closed slurry inlet) was also predicted to boil; however, the jet of water in this case had a very high speed (645 m/s, predicted by CFD modeling [15]) as it flowed directly down the mixing tube without any wall contact. Therefore, a given segment of the jet traveled through the mixing chamber and mixing tube in just 17 ms, which was assumed to be too short an interval to establish boiling. Therefore, the water-only jet remained thin and did not diverge, as seen in Fig. 2. Boiling thus only occurred in the slurries since they moved relatively slowly within the mixing chamber.

The mixing chamber pressure is seen to increase in Fig. 6 with increasing slurry tube size. The additional slurry entering the mixing chamber produced larger reductions in the jet velocity, as discussed in part II of this paper, thus reducing the strength of the partial vacuum in the chamber. The two largest slurry tubes, 3.08 and 4.51 mm^2, were predicted to completely flood the mixing chamber while operating at 233 MPa, as indicated in Fig. 5. Figure 6 shows that the mixing-chamber pressure for both tube sizes was approximately atmospheric.

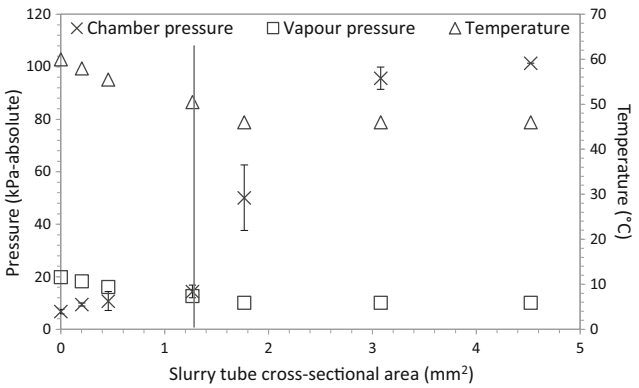

Fig. 6 Mixing chamber pressure and temperature as a function of slurry tube size for a pump pressure of 233 MPa. Also shown for reference are the vapor pressure of water at the corresponding temperature of the jet and the predicted boiling condition represented by the vertical line. Tube size of zero corresponds to the blocked slurry inlet. Scatter bars represent ±1 standard deviation from four separate tests. Scatter bars for temperature readings were all small enough to fit within the symbols

This explains why the slurry flow rate was so low for these tube sizes in Fig. 5, since a fully-flooded mixing chamber was incapable of producing a partial vacuum within the chamber and so the effective pressure-head driving the slurry flow was greatly reduced. Thus, the pressure measurements of Fig. 6 are consistent with the predicted flooding condition of Fig. 5.

4.2.2 Jet diameter

The jet exiting the mixing tube in AWJM diverges because it contains air that entered the mixing chamber with the abrasive, as discussed by Haghbin et al. [12]. It was hypothesized that boiling within the mixing chamber in HASJM generated vapor that would be entrained by the jet and also cause it to diverge. This divergence due to vapor entrainment would be in addition to that caused by the entrainment of the slurry. This was investigated by using a solution of 30 wt% ethylene glycol and 70 wt% water in place of the aqueous slurry in order to decrease the mixture vapor pressure and prevent boiling under conditions that would boil a purely aqueous slurry. This mixture had a boiling point of 122 °C at atmospheric pressure and a vapor pressure of 9.7 kPa at 50 °C. The ethylene glycol also increased the viscosity of the solution; however, Kowsari et al. [26] reported that viscosity had no significant effect on the jet diameter. Figure 7 shows that with the 0.46 mm^2 slurry tube and a pump pressure of 233 MPa, conditions which produced boiling (Fig. 6), the jet formed with the ethylene glycol solution did indeed have a smaller diameter at a given standoff distance than did the jet formed when pure water entered the mixing chamber via the slurry tube (no abrasive was used in either jet). This supports the hypothesis that boiling in the mixing chamber generated significant amounts of water vapor that became entrained in the jet and caused greater jet divergence.

This experiment was repeated using a saturated solution of NaCl in water with a boiling point of 108 °C at atmospheric pressure and a vapor pressure of 11.1 kPa at 50 °C. Water, having the lowest boiling point of the three mixtures, was expected to produce the most vapor and create the largest jet diameter. The jet of the ethylene glycol mixture was expected to spread the least since it cannot boil. The jet diameters for the three solutions are shown in Fig. 8, and were obtained from the widths of the machining cuts in the foam board using a slow traverse speed of 10 mm/min and a large standoff distance of 5 mm. Three repeat cuts were made for each of the three mixtures in each of the six tube sizes for a total of 54 experiments. Each cut width was measured at eight locations along the cut for a total of 432 data points in Fig. 8.

The tube sizes greater than the solid vertical water-boiling line in Fig. 8 were predicted not to cause boiling for the water slurry, and thus the other mixtures as well, according to Fig. 6. In these cases, the jet divergence was determined solely by the mixing with the slurry. Consistent with this hypothesis, the

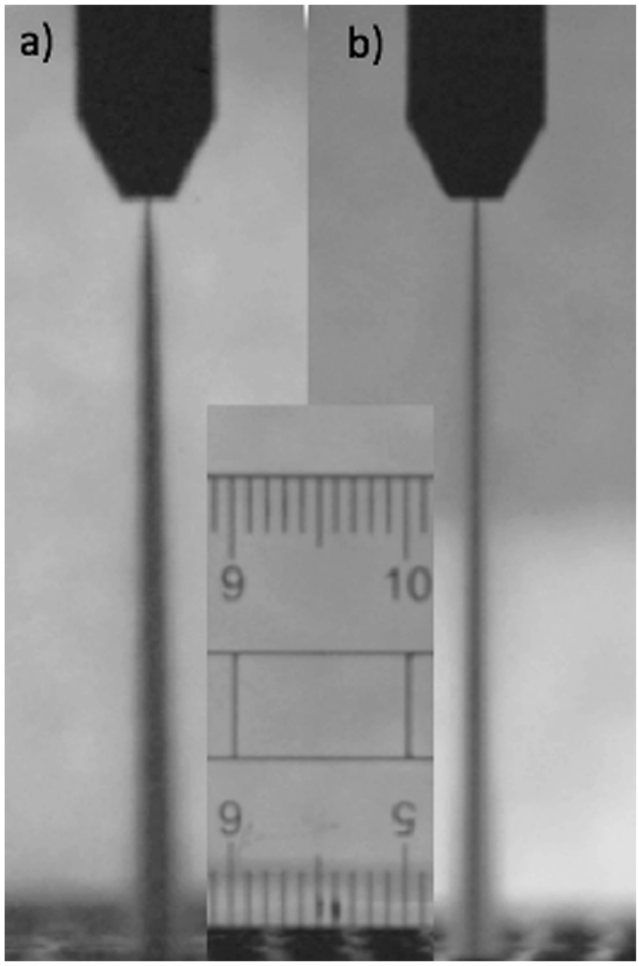

Fig. 7 Images of jets generated with the 0.46-mm^2 slurry tube: (**a**) Slurry tube carried only water, and (**b**) slurry tube carried only ethylene glycol solution. Both images were taken with a pump pressure of 233 MPa, which would cause slurry water to boil inside the mixing chamber. Scale in mm

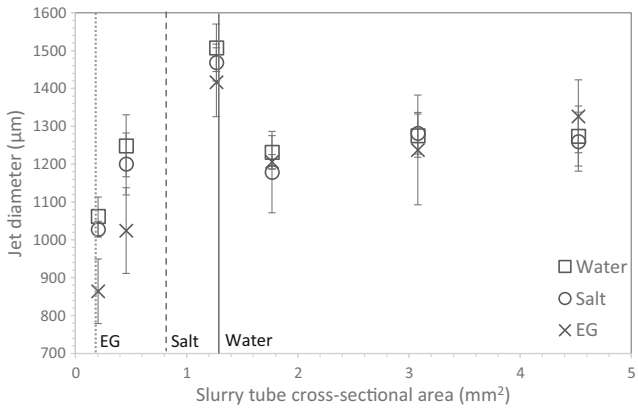

Fig. 8 The effect of boiling on jet diameter while entraining solutions with three different boiling points in the mixing chamber. The solid, dashed, and dotted vertical lines represent the boiling condition for water, the salt solution, and the ethylene glycol (EG) mixture, respectively, for a pump pressure of 233 MPa (respective points to the left of each line predicted to boil). Scatter bars represent ±1 standard deviation from three separate tests for each mixture and for each slurry tube size

three liquids with these larger tubes produced very similar jet diameters, with differences that were statistically insignificant at the 95% confidence level (*t* tests), except for the 1.77 mm^2 slurry tube between the salt solution and the water data points, where the confidence was 90%.

The jet diameter for the three smallest tube sizes (0.2, 0.46, 1.27 mm^2) in Fig. 8 increased with tube size for all three liquids because more slurry was entrained with increasing tube size. However, in addition to this effect of the slurry mixing with the high-speed jet, Fig. 6 shows that these three tubes were predicted to cause boiling of pure water within the mixing chamber. As expected by the hypothesis that this additional water vapor would cause greater jet divergence, Fig. 8 shows that, for each of the three tubes, the jet diameters did indeed increase as the amount of boiling was predicted to increase; i.e., for a given tube size the jet diameter increased in the order of the vapor pressure at the chamber temperature: water > salt solution > ethylene glycol solution. Moreover, for the three smallest tube sizes (those that boiled water), the differences in the jet diameter between the ethylene glycol solution (which did not boil) and the jets of both water and the salt solution, decreased as the amount of boiling decreased with increasing slurry tube size. For the three smallest slurry tube sizes that caused water in the mixing chamber to boil (Fig. 6), *t* tests showed that there were statistically significant differences between the jet diameter means for all mixture combinations, except between the salt water and water data points with the 1.27-mm^2 tube, where the significance level was 90%. Overall, Fig. 8 supported the hypothesis that jet divergence increased in proportion to the level of vapor production due to boiling in the mixing chamber.

5 Conclusions

A water jet machine was modified to permit various abrasive slurries to enter the mixing chamber in place of the usual air and abrasive. The slurry flow rate into the mixing chamber of this high-pressure abrasive slurry-jet was controlled accurately over a wide range of particle concentrations by changing the size of the slurry inlet tubes and the elevation of the slurry reservoirs. The slurry mass flow rate for a given water jet pump pressure increased as the tube size increased until the mixing-chamber became flooded with slurry. For pump operating pressures of 134 and 233 MPa, the smallest tube sizes that caused the mixing chamber to flood were 1.27 mm^2 and 1.5 mm^2, respectively. At this point the rate of slurry inflow exceeded the maximum possible outflow caused by entrainment by the high-velocity water jet. This fully-flooded condition caused a large decrease in the slurry flow rate as the pressure within mixing chamber became approximately equal to atmospheric pressure. The minimum slurry mass flow rate that caused flooding of the mixing chamber was dependent on the pump operating pressure, ranging from 60 g/min to 200 g/min for pump operating pressures of 134 and 233 MPa, respectively. At this point, the high-velocity water jet from the water jet orifice became a submerged jet as it entered the flooded mixing chamber and was decelerated by fluid drag.

Prior to the fully-flooded condition, with smaller slurry tubes and slurry flow rates, the high-velocity water jet created a partial vacuum within the mixing chamber, thereby drawing slurry into the chamber. Mixing chamber pressure and temperature measurements showed that boiling could occur under these conditions. The water vapor generated by the boiling caused the jet diameter to increase, as inferred from the widths of cuts in a polymeric foam-board. These results were consistent with the trends observed in additional experiments using mixtures with higher boiling points made with the addition of salt or ethylene glycol. By avoiding the boiling condition, narrower cuts were made.

The control of the slurry flow rate using slurry tubes with varying sizes also permitted the use of slurries with high particle concentrations without clogging. This increased the erosion rate, and a minimum particle concentration of 17 wt% made it possible to machine holes in glass without cracking or chipping.

Part II of this work [15] presents a CFD model of the flows within the mixing chamber that is used to predict the velocity and erosive performance of the slurry jet exiting the mixing tube. These predictions are then compared with measured rates of machining on aluminum workpieces.

Funding information The authors acknowledge the financial support of the Natural Sciences and Engineering Research Council of Canada (NSERC), and the Canada Research Chairs Program.

References

1. Kowsari K, Sookhaklari MR, Nouraei H, Papini M, Spelt JK (2016) Hybrid erosive jet micro-milling of sintered ceramic wafers with and without copper-filled through-holes. J Mater Process Technol 230:198–210
2. Liu HT (2010) Waterjet technology for machining fine features pertaining to micromachining. J Manuf Process 12(1):8–18
3. Liu HT (2017) Precision machining of advanced materials with waterjets. IOP conference series: mater. Sci Eng 164(1):012008
4. Nguyen T, Pang K, Wang J (2009) A preliminary study of the erosion process in micro-machining of glasses with a low pressure slurry jet. Key Eng Mater 389:375–380
5. Wang J, Nguyan T, Pang K (2009) Mechanism of microhole formation on glasses by an abrasive slurry jet. J Appl Phys 105(4): 044906
6. Pang K, Nguyen T, Fan JM, Wang J (2010) Machining of microchannels on brittle glass using an abrasive slurry jet. Key Eng Mater 443:639–644

7. Humphrey J (1990) Fundamentals of fluid motion in erosion by solid particle impact. Int J Heat Fluid Fl 11:170–195
8. Nouraei H, Wodoslaysky A, Papini M, Spelt JK (2013) Characteristics of abrasive slurry jet micro-machining: a comparison with abrasive air jet micro-machining. J Mater Process Technol 213(10):1711–1724
9. Liu, H. T. (1998). Near-net shaping of optical surfaces with abrasive suspension jets. 14th Int. Conference on Jetting Technology, Brugge, 285–294
10. Hashish M (1993) Performance of high-pressure abrasive suspension jet system. Am Soc Mech Eng 67:199–207
11. Miller DS (2004) Micromachining with abrasive waterjets. J Mater Process Technol 149(1–3):37–42
12. Haghbin N, Ahmadzadeh F, Spelt JK, Papini M (2015) Effect of entrained air in abrasive water jet micro-machining: reduction of channel width and waviness using slurry entrainment. Wear 344-345:99–109
13. Haghbin N, Spelt JK, Papini M (2015) Abrasive waterjet micro-machining of channels in metals: comparison between machining in air and submerged in water. Int J Mach Tools Manuf 88:108–117
14. Haghbin N, Ahmadzadeh F, Spelt JK, Papini M (2016) High pressure abrasive slurry jet micro-machining using slurry entrainment. Int J Adv Manuf Technol 84(5–8):1031–1043
15. Teti, M., Spelt, J. K., Papini, M. (submitted). Jet properties and mixing chamber flow in a high-pressure abrasive slurry jet: part II- machining rates and CFD modeling. Int J Adv Manuf Technol
16. Leu MCP, Geskin ES, Tismeneskiy L (1998) Mathematical modeling and experimental verification of stationary waterjet cleaning process. J Manuf Sci Eng 120:571–579
17. Huang L, Folkes J, Kinnel P, Shipway PH (2012) Mechanisms of damage initiation in a titanium alloy subjected to water droplet impact during ultra-high pressure plain waterjet erosion. J Mater Process Technol 212(9):1906–1915
18. How does a waterjet work. OMAX abrasive water jet cutting machine, (1993). Kent, WA, USA, https://www.omax.com/learn/how-does-waterjet-work
19. ASTM C702-98 (2003). Standard practice for reducing samples of aggregate to testing size. American Society for Testing and Materials (ASTM), http://www.astm.org/database.cart/historical/C702-98R03.htm
20. International alloy designations and chemical composition limits for wrought aluminum and wrought aluminum alloys (2015), The Aluminum Association, 1525 Wilson Boulevard, Arlington, VA 22209, USA. www.aluminum.org
21. Borofloat 33 – general information. SCHOTT Technical Glass Solutions. Louisville, KY, USA, https://www.schott.com/d/borofloat/b2c50cc4-74a1-4c31-8af3-c7de01877182/1.0/borofloat33_gen_eng_web.pdf
22. Borofloat 33 – mechanical properties. SCHOTT Technical Glass Solutions. Louisville, KY, USA, https://www.schott.com/d/borofloat/723d30c8-cca0-4159-ad40-31e658dbf588/1.0/borofloat33_mech_eng_web2.pdf
23. ASM Handbook, Volume 2 – Properties and selection: nonferrous alloys and special-purpose materials. ASM International Handbook Committee, (2010). Geauga County, OH, USA, https://app.knovel.com/web/view/khtml/show.v/rcid:kpASMHVP07/cid:kt007OVTL2/viewerType:khtml/?view=collapsed&zoom=1&page=8
24. Liu HT, Schubert E (2008) Piercing in delicate materials with abrasive-waterjets. Int J Adv Manuf Technol 42:263–279
25. Schwartzentruber J, Papini M (2014) Abrasive waterjet micro-piercing of borosilicate glass. J Mater Process Technol 219:143–154
26. Kowsari K, Nouraei H, James DF, Spelt JK, Papini M (2014) Abrasive slurry jet micro-machining of holes in brittle and ductile materials. J Mater Process Technol 214(9):1909–1920